Anatomical Registration and Segmentation by Warping Template Finite Element Models

Anton E. Bowden[1], Richard D. Rabbitt[1], and Jeffrey A. Weiss[1,2]

[1]Department of Bioengineering, University of Utah Salt Lake City, UT 84112-9202
[2]Orthopedic Biomechanics Institute, The Orthopedic Specialty Hospital, SLC, UT 84107

ABSTRACT

Image segmentation and anatomical registration play an important role in subject-specific computational modeling and image analysis. Often a three-dimensional (3D) segmentation is available for a canonical *template* image dataset of a single subject. The goal of the present work is to apply this *apriori* knowledge to facilitate segmentation of anatomical structures in other subjects. A "Warping" method was developed to deform the template anatomy and register it with specific *target* anatomies. This was achieved by direct incorporation of image data into a nonlinear finite element (FE) analysis program. The algorithm searches all admissible material configurations for the one which minimizes the difference between the target and the deformed template. FE models of specific anatomical structures were generated from the anatomy of one specific template subject. The FE model deforms under the laws of nonlinear continuum mechanics such that one-to-one correspondence of differential lines, areas, and volumes is guaranteed. The method has been successfully applied to 2D and 3D segmentation, registration, and geometrical model construction. Example results are provided for segmentation of the distal femur using X-ray computed tomography (CT) data, and registration of neuroanatomical structures using optical cryosection image data.

Keywords: nonlinear kinematics, tissue and organ segmentation, inter-subject registration, geometrical model generation, anatomical warping, global shape models

1. INTRODUCTION

Semi-automatic and automatic template-based registration techniques have been applied to a broad spectrum of uses in fields such as handwriting recognition,[1,2] vehicle classification,[3] facial feature recognition,[4] military target identification, manufacturing,[5] and nonlinear strain computation.[6] The principal use of such techniques to date is medical image segmentation and registration. The motivation for the use of deformable templates to automatically register and segment medical image data lies in the considerable human effort required to achieve these tasks manually. Manual segmentation is a painstaking process of selecting points within an image data set which lie on the boundaries of a region of interest (ROI). For many applications, the ROI must be identified on each slice of a 3D data set. Similar procedures are used in manual comparison of functional image data with a reference or atlas. Landmarks within a data set must be manually identified so that information from a specific patient data set can be transformed to a reference or template space. An example of this is the transformation of cortical information into the Talairach-Tournoux[7] space.

Recent attempts to automate the segmentation procedure using deformable templates have followed three distinct lines. Landmark or marker based identification techniques attempt to automatically align key points from a template image set with those in a target data set.[8] Principal Axis registration methods are based on low-dimensional translation, rotation, and scaling operations.[9,10] The third area of research is the more diverse field of deformable shape models. When these methods are rigorously applied, the template transformation is governed by principles of nonlinear differential geometry or continuum mechanics. Some methods focus on border information, such as the deformable contour models of Cohen.[11] Others have used full volumetric approaches using linear solid mechanics,[12] fluid mechanics,[13] or nonlinear continuum mechanics.[14]

Further author information:
A.E.B.(correspondence): Email: Anton.Bowden@m.cc.utah.edu; Telephone: 801-581-4549
R.D.R.: Email: R.Rabbitt@m.cc.utah.edu; Telephone: 801-581-6968
J.A.W.: Email: jeff@usi.utah.edu; Telephone: 801-269-4035

The present work applied the techniques described by Rabbitt, et. al.[14,6] to deform a discretized geometric representation of a 3D template data set subject to the laws of nonlinear continuum mechanics. This method required the solution of a nonlinear optimization problem to minimize the difference between target images collected from the subject of interest and images formed by mathematical interrogation of a deformed finite element (FE) model.

Two examples are presented. The first illustrates the ability to segment regions of the Macaque monkey brain using inter-subject registration of optical cryosection data. In the second example, CT data was used to register a 3D template model of the distal femur with a second subject. Results provide subject-specific tissue segmentation and FE mesh generation.

2. METHODS

2.1. Mathematical Basis

Only a descriptive outline of the mathematical basis of the method is presented here. For a more thorough treatment of the derivation, please refer to Rabbitt.[14,6] Briefly, using standard techniques from continuum mechanics, a deformation map φ was defined which related a reference configuration with material coordinates $\mathbf{X}$ to a target configuration with mapped material coordinates $\mathbf{x}$. A hyperelastic material model was used such that a strain energy density function $W(\mathbf{X}, \mathbf{C}(\varphi))$ was defined, where $\mathbf{C}(\varphi)$ is the right Cauchy strain tensor.[15] In addition to the strain energy density function, a Gaussian image-based energy density function $U(\mathbf{X}, \varphi)$ was used to relate the mathematically interrogated spatial information from the template to the target data.[13] Both energy terms were incorporated into a combined energy density functional:

$$E(\varphi) = \int_\beta W(\mathbf{X}, \mathbf{C}(\varphi(\mathbf{X})))dV + \int_\beta U(\mathbf{X}, \varphi(\mathbf{X}))dV \tag{1}$$

which was used to derive the weak form of the Euler-Lagrange equations. The domain of the template space was discretized and the FE method was used to survey all possible template configurations and select the one which minimized the combined energy functional. When solved using the penalty method,[16] this is equivalent to a Bayesian approach, where W defines the Gibbs form of the prior probability and U defines the likelihood.

2.2. Implementation

Solution of the problem is divided into three steps: preprocessing, processing, and postprocessing. In the preprocessing step, a geometric model is constructed, boundary conditions are specified, and material properties are assigned. The geometric model must span the ROI of the template image. In some cases it is necessary to histogram equalize the template and target images to correct for differences between scanners and data collection techniques. Figure 1 shows histograms from two image data sets. Differences such as these were accommodated by simply averaging the mean and amplitude of the histogram according to:

$$x^* = x\frac{\overline{x_1}}{\overline{x_2}}; \quad x \leq \overline{x_2} \tag{2}$$

$$x^* = (x - \overline{x_2})\frac{x_{max} - \overline{x_1}}{x_{max} - \overline{x_2}} + \overline{x1}; \quad x > \overline{x_2} \tag{3}$$

$$I_2^* = I_2\frac{\overline{I_1}}{\overline{I_2}} \tag{4}$$

$$I_2^{**}(x) = I_2^*(x^*) \tag{5}$$

where I is an index along the histogram (e.g. 0 to 255), and x is the frequency of occurrence of a particular intensity within the image.

The combined energy functional was minimized during the processing step by implementing equation 1 into the nonlinear finite element code NIKE3D.[17,6] Use of such a well-developed finite element package allowed for broad variation in both applied boundary conditions and material constitutive parameters which can be used to guide the registration process. It also allowed independence of the computational mesh from the spatial discretization of the

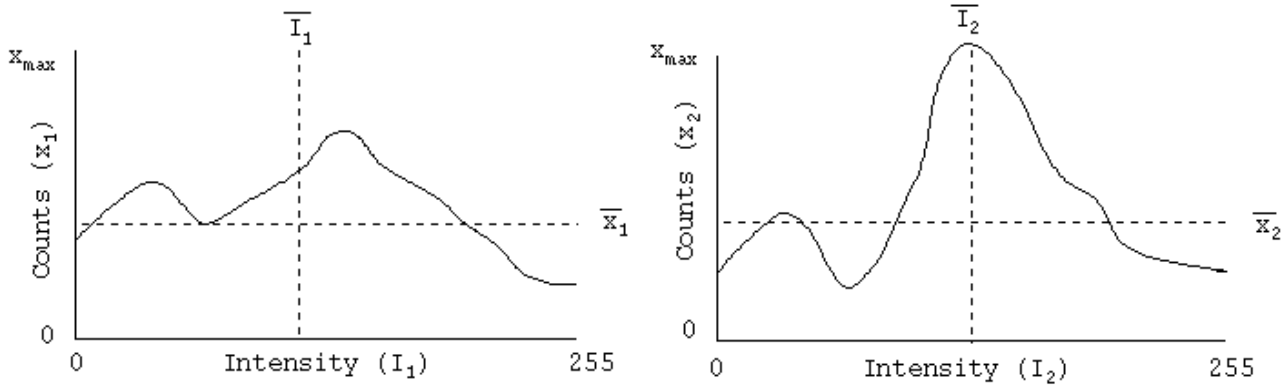

Figure 1. Description of a histogram equalization process. The equations governing the histogram transformation are given in (2)-(5)

image data. This independence can be important in reducing the computational size of the geometrical model and in cases where the ROI does not include an entire image data set. Template and target images are interpolated from voxel coordinates to the FE model to define a continuous mathematical representations of the data. These representations are updated as the material deforms through the spatially fixed image coordinates. Differences between intensity of the target and template images, as well as their gradients, contribute a spatially dependent body force which drives the registration process. These differences also contribute to the tangent stiffness in the FE implementation.

Field variables, including displacement, relative volume, and strain, were viewed using the postprocessor GRIZ.[18] Additional postprocessing software was written to output the deformed template as an image data set. This required interpolation of Lagrangian displacements to generate pixel locations and intensities within the Eulerian image-based coordinate frame. If the registration were perfect, subtraction of the deformed template from the target image would result in a zero difference image. Thus, visual inspection of the difference image provides a qualitative means to assess the registration.

3. RESULTS

3.1. 2D neuroanatomical slices

Results appearing previously in the literature for neuroanatomical registration often use rectangular computational grids associated with image voxels.[12,13] The present FE method allows for both rectangular and irregular mesh structure. This technique was applied to segment grey matter, white matter, and sulci of macaque monkey brains using optical images of stained cryosection slices. Results are provided for three different computation meshes: a simple regular mesh, a mesh conforming to a lobe of grey and white matter, and a mesh conforming to a layer of grey matter. In all cases, the material was modeled as an elastic-plastic solid with a low Poisson's ratio.[17] Deformation of the template brain slice was constrained to the plane of the image data.

3.1.1. Rectangular Mesh

Figure 2 provides results for a simple rectangular mesh constructed to span the domain of the image data. The outside edges of the mesh were aligned with the borders of the images and constrained from both vertical and horizontal motion. The template image is shown in panel A and the target image is shown in panel E. The goal is to find the deformation of the FE mesh (B) that aligns the deformed template with the target (E). Prior to deformation the difference image (Template-Target,C), contains regions of large magnitude intensities. After minimizing the functional (equation 1), the difference image is reduced from (C) to (D). The displacement magnitude (F), maximum shear strain (G), and relative volume (H) associated with the deformation are also shown. The final deformed

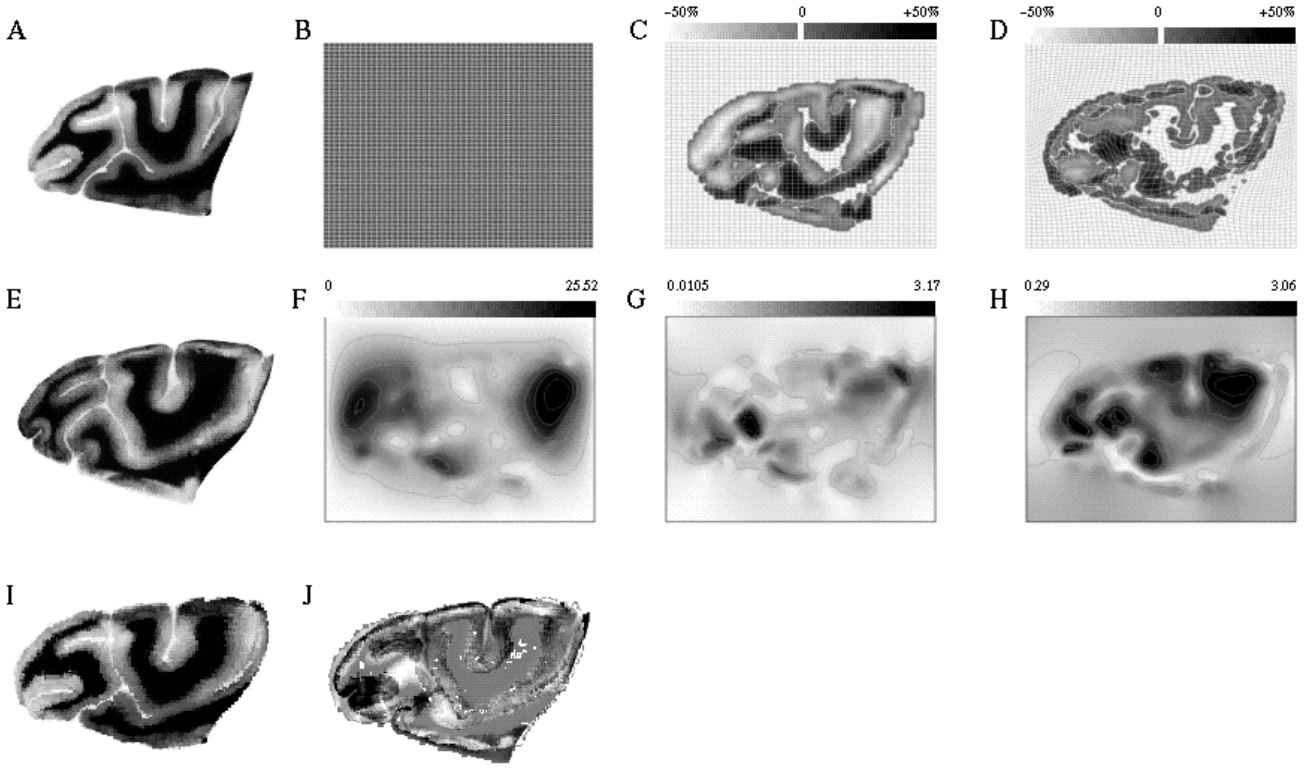

Figure 2. Regular mesh results. A) Template image. B) Computational mesh. C) Intensity difference before registration. D) Intensity difference after registration. E) Target image. F) Computed displacement magnitude. G) Computed principle shear strain. H) Computed relative volume. I) Deformed template image. J) Relative error. In F-H, the greyscale legend is given above each panel. Percent values in C-D correspond to the percentage of maximum initial difference in image intensity.

template, mapped to the image voxels, is shown in the lower left panel (I). Accuracy of spatial location in the segmentation is shown in the final difference image (E-I) in panel J. Note the large differences in location of sulci between the target (E) and the deformed template (I). These results represent a local minima in the energy function and are not considered acceptable.

3.1.2. Lobe Mesh

Better results were obtained using geometrical FE models that align with specific anatomical structures. Figure 3 provides results for an irregular mesh (B) constructed to span the white and grey matter between the central and rightmost sulci. No external boundary conditions were applied, so the edges of the mesh were free to move. Panels A-J correspond directly with those in figure 2. In both cases, results are computed on the geometrical model and thus are not available outside the spatial domain of the mesh. The registration results are much more acceptable with reference to both the difference in image intensity following registration (D) and the global positioning of the deformed template (I-J). The undeformed FE mesh is a segment of the template anatomy. The deformed mesh aligns well with the same region of the brain in the target anatomy, illustrating automatic segmentation.

3.1.3. Grey Matter Mesh

Figure 4 provides results for a FE mesh corresponding to a section of grey matter. Again the panels correspond to those shown in figure 2. Note the large volume changes associated with this registration (H). The difference in image intensity following the registration (D) has almost been reduced to zero. Automatic segmentation is demonstrated by the difference image (J) where the deformed FE mesh overlays the grey matter of the target.

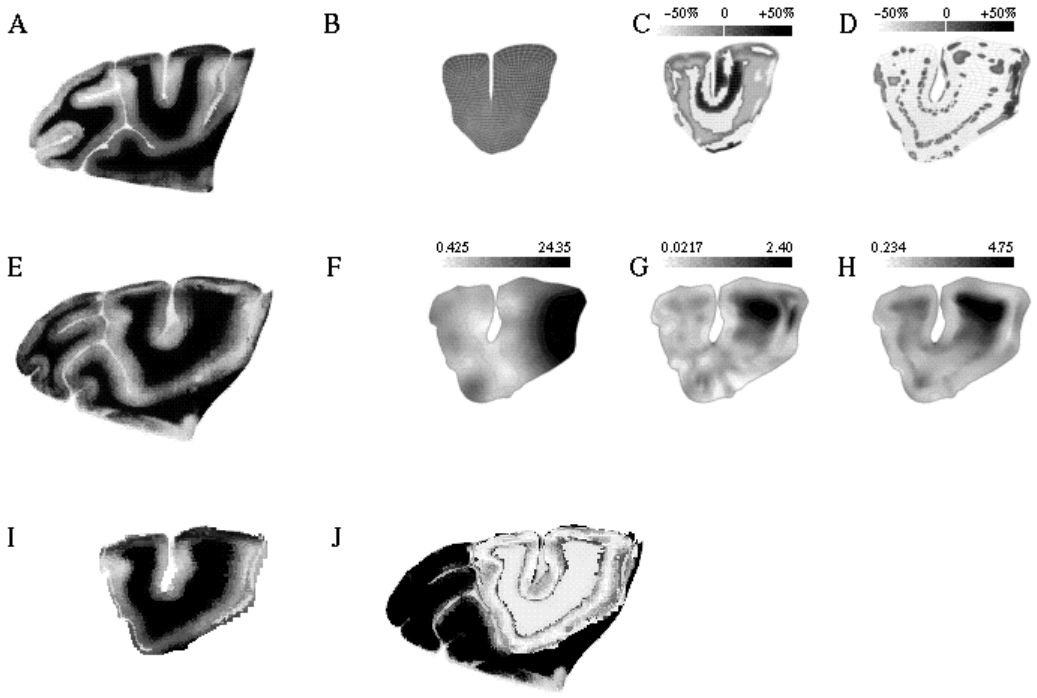

Figure 3. Center section results. Same notation as in figure 2.

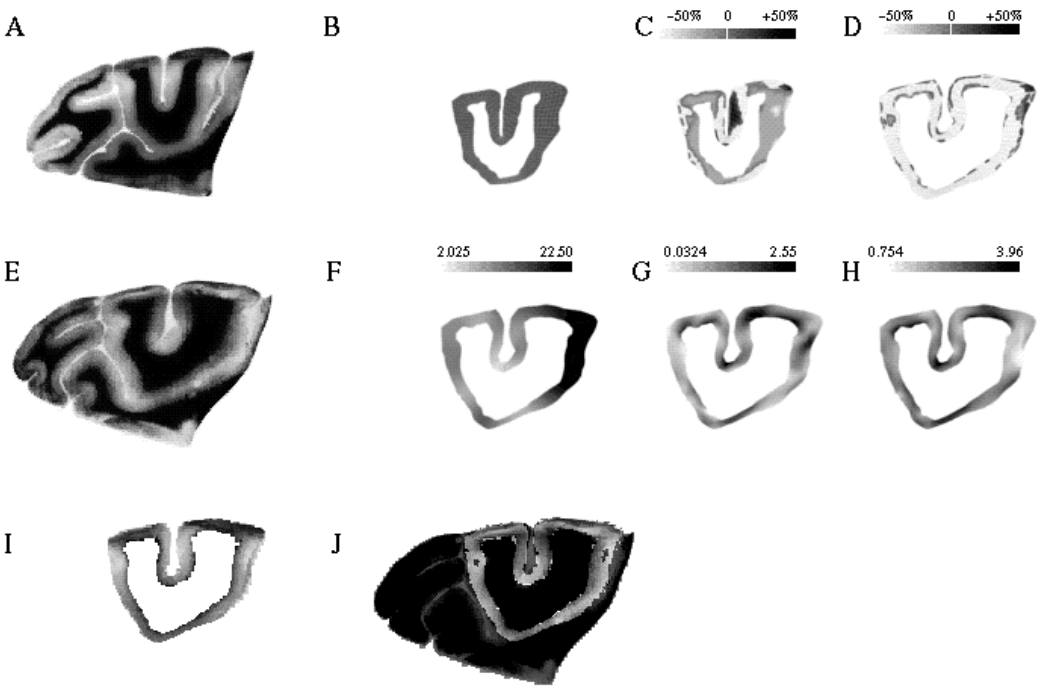

Figure 4. Grey matter results. Same notation as in figure 2.

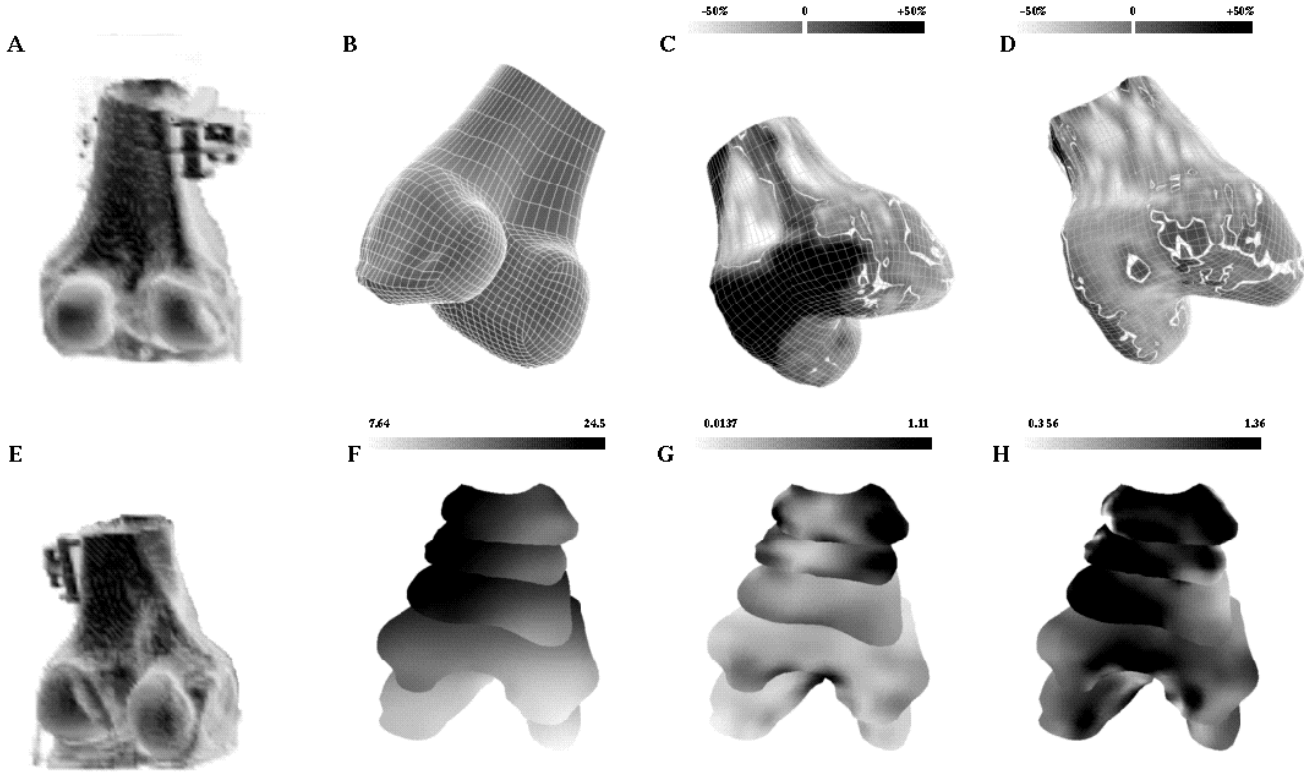

Figure 5. 3D femur results. A) Template data set. B) Template mesh. C) Intensity difference before registration. D) Intensity difference after registration. E) Target data set. F) Computed displacement magnitude. G) Computed principle shear strain. H) Computed relative volume.

3.2. 3D human femur

The method can also be applied to generate subject specific geometric models – a problem equivalent to tissue segmentation. This is illustrated in figure 5 where a FE model, generated from the CT data of one subject (template), is mapped to a second subject (target). Panels A and E show rendered views of the 3D CT data corresponding to the template and target respectively. The template FE mesh used for the registration is shown in panel B. Subtraction of the target CT image data from the deformed template generates a difference image. Values of the difference image are shown on the surface of the femur model before (C) and after (D) registration. Deformation results are presented on parallel slices through the long axis of the femur (F-H): displacement magnitude (F), maximum shear strain (G), and relative volume (H). The difference between the reference geometry (C) and the deformed configuration (D) is the result of rigid body translation and rotation, as well as fine scale deformation. Note the elongation and torsion induced on the mesh configuration (*cf.* C,D).

4. DISCUSSION

During image segmentation and registration, template and target images are typically taken from different subjects and hence the mapping is not a physical deformation. Rather, the mapping represents the optimal configuration that aligns the template and target data. Use of nonlinear continuum mechanics in the process guarantees a one-to-one mapping of differential lines, areas, and volumes between the template and its deformed configuration. This is required to insure that anatomical structures in the template remain continuous after the deformation. Paradoxically, this strength is sometimes a weakness in that strict adherence to the laws of mechanics can overpenalize some deformation fields. The severity depends upon the material properties used. In the registration problems we have

run to date, acceptable results were obtained by *ad hoc* manual selection of material properties. Optimization of material parameters for anatomical registration remains a topic of future work.

The neuroanatomical registration results illustrate the difference in segmentation results achieved by a rectangular mesh versus a mesh corresponding to the tissue geometry. The rectangular mesh achieved unacceptable results because of the presence of a local minimum in the combined energy functional (equation 1). Experience has shown that local minima are more likely to occur during 2D segmentations on rectangular grids due to competing regions in the image data. Meshing only the ROI using an irregular mesh not only avoided such phenomena, but also reduced the computational size of the problem. An additional advantage to the irregular FE mesh was the direct segmentation afforded by the deformed template image (Panel I in figures 3 and 4). Although segmentation information could be extracted from the displacement field of a rectangular mesh, the transformation is not as obvious.

The 3D capabilities of the present method are demonstrated in the distal femur registration. In 3D segmentations, the independence of the computational mesh from the voxel space of the image data is especially relevant. A small ROI in a data set can be extracted without the computational burden of the bringing the whole image space into registration. This example further illustrates an important aspect of the present FE method. Considerable effort is required to construct structured computational meshes that accurately reflect the tissue geometry. The distal femur registration demonstrates a convenient way to automatically generate complex computational meshes by mapping a canonical template model to conform with the anatomy of an individual subject.

ACKNOWLEDGEMENTS

The finite element mesh and the computed tomography data used in the 3D femur registration were provided by John C. Gardiner of the Orthopedic Biomechanics Institute, Salt Lake City, UT. Cryosection data was provided by D. C. Van Essen of Washington University, St. Louis, MO. Partial support for this project was provided by the University of Utah Research Foundation, the University of Utah Center for High Performance Computing and the Human Brain Project (NIMH, NSF and NASA RO1 MH/DA52158).

REFERENCES

1. E. Lecolinet and L. Likforman-Sulem, "Handwriting analysis: Segmentation and recognition," *IEE Colloq Proc Eur Wkshp Handwriting Anal Recog: A European Perspective* **123**, pp. 17/1–17/8, 1994.
2. A. del Bimbo, S. Santini, and J. Sanz, "OCR from poor quality images by deformation of elastic templates," in *Proc Int Conf Pattern Recognit*, vol. 2, pp. 433–435, Oct 1994.
3. M. P. Dubuisson, S. Lakshmanan, and A. K. Jain, "Vehicle segmentation using deformable templates," in *Int Symp Comp Vision*, International Symposium – Coral Gables, FL, pp. 581–586, IEEE; Computer Society; Technical Committee for Pattern Analysis and Machine Intelligence, IEEE, Nov 1995.
4. K. Lam and H. Yan, "Facial feature location and extraction for computerized human face recognition," *Natl Conf Pub Inst Eng Aust* **1(94/9)**, pp. 167–171, 1994.
5. C. Gueudre, J. Moysan, and G. Corneloup, "Geometric characterization of a circumferential seam by automatic segmentation of digitized radioscopic images," *NDT & E International* **30**(5), pp. 279–285, 1997.
6. J. Weiss, R. Rabbitt, and A. Bowden, "Incorporation of medical image data in finite element models to track strain in soft tissues," *SPIE Biomed Optics Symp BiOS98* **3254**, 1998.
7. J. Talairach and P. Tournoux, "Co-planar stereotaxic atlas of the human brain," *Stuttgart, Germany:* **Thieme**, 1988.
8. Y. Amit, "Graphical shape templates for automatic anatomy detection with applications to MRI brain scans," *IEEE Trans Med Imaging* **16**, pp. 28–40, Feb 1997.
9. L. K. Arata, D. A. P., J. P. Broderick, M. F. Gaskil-Shipley, A. V. Levy, and N. D. Volkow, "Three-dimensional anatomical model-based segmentation of MR brain images through principal axis registration," *IEEE Trans Biomed Engineering* **42**, pp. 1069–1077, Nov 1995.
10. A. P. Dhawan, L. K. Arata, A. V. Levy, and J. Mantil, "Iterative principal axis registration method for analysis of MR-PET brain images," *IEEE Trans Biomed Engineering* **42**, pp. 1069–1077, Nov 1995.
11. L. Cohen and R. Kimmel, "Global minimum for active contour models: A minimal path approach," *Int J Comp Vision* **24**(1), pp. 57–78, 1997.

12. R. Bajcsy, R. Lieberson, and M. Reivich, "A computerized system for the elastic matching of deformed radiographic images to idealized atlas images," *J Comp Assist Tomography* **7**(4), pp. 618–625, 1983.
13. G. E. Christensen, R. D. Rabbitt, and M. Miller, "Deformable templates using large deformation kinematics," *IEEE Trans Image Process* **5**(10), pp. 1435–1447, 1996.
14. R. Rabbitt, J. Weiss, G. Christensen, and M. Miller, "Mapping of hyperelastic deformable templates," in *Proc Int Soc Optical Engineering*, vol. 252, pp. 252–265, SPIE, 1995.
15. A. Spencer, *Continuum Mechanics*, Longman Scientific & Technical, Essex, England, 1980.
16. K.-J. Bathe, *Finite Element Procedures*, Prentice-Hall, Englewood Cliffs, New Jersey, 1996.
17. B. Maker, R. Ferencz, and J. Hallquist, "NIKE3D a nonlinear, implicit, three-dimensional finite element code for solid and structural mechanics," *UC - Lawrence Livermore National Laboratory Report* **UCRL-MA-105268 rev 1**, 1995.
18. D. Dovey and T. Spelce, "GRIZ finite element analysis results visualization for unstructured grids," *UC - Lawrence Livermore National Laboratory Report* **UCRL-MA-115696**, 1993.